Chemical Science

Accepted Manuscript

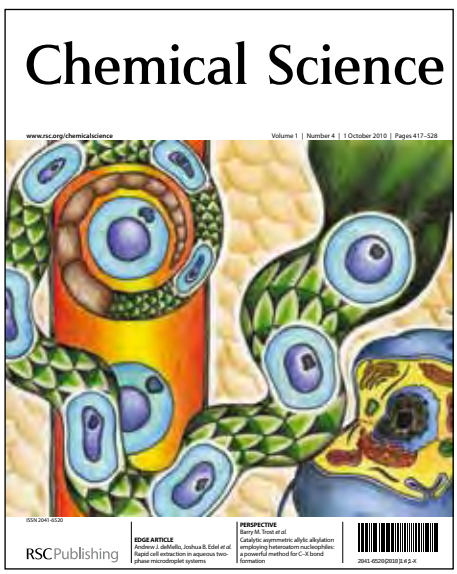

This is an *Accepted Manuscript*, which has been through the RSC Publishing peer review process and has been accepted for publication.

Accepted Manuscripts are published online shortly after acceptance, which is prior to technical editing, formatting and proof reading. This free service from RSC Publishing allows authors to make their results available to the community, in citable form, before publication of the edited article. This *Accepted Manuscript* will be replaced by the edited and formatted *Advance Article* as soon as this is available.

To cite this manuscript please use its permanent Digital Object Identifier (DOI®), which is identical for all formats of publication.

More information about *Accepted Manuscripts* can be found in the **Information for Authors**.

Please note that technical editing may introduce minor changes to the text and/or graphics contained in the manuscript submitted by the author(s) which may alter content, and that the standard **Terms & Conditions** and the **ethical guidelines** that apply to the journal are still applicable. In no event shall the RSC be held responsible for any errors or omissions in these *Accepted Manuscript* manuscripts or any consequences arising from the use of any information contained in them.

Chemical Science

RSCPublishing

ARTICLE

Ground and Excited State Electronic Spectra of Perylenediimide Dimers with Flexible and Rigid Geometries in DNA Conjugates†

Prakash P. Neelakandan, Tarek A. Zeidan, Martin McCullagh, George C. Schatz, Josh Vura-Weis, Chul Hoon Kim, Michael R. Wasielewski and Frederick D. Lewis*

Cite this: DOI: 10.1039/x0xx00000x

Received ooth January 2012,
Accepted ooth January 2012

DOI: 10.1039/x0xx00000x

www.rsc.org/

The structure and electronic spectra of six DNA conjugates possessing two face-to-face perylenediimide (PDI) chromophores have been investigated. Structures of hairpins possessing two adjacent PDI base analogues opposite a tetrahydrofuran abasic site on the same or opposite strands were simulated using molecular dynamics. These structures are compared with those previously reported for a duplex and hairpin dimer possessing PDI linkers. The minimized structures all have face-to-face PDI geometries but differ in the torsional angle between PDI long axes and the offset between PDI centers. These structures provide the basis for analysing differences in the electronic spectra of the PDI dimers both in the ground state (UV-Vis and circular dichroism spectra) and excited state (fluorescence and transient absorption) determined in aqueous buffer and in the denaturing solvent dimethyl sulfoxide. PDI dimers with rigid structures and large PDI-PDI torsional angles display large effects of exciton coupling in their UV-Vis and CD spectra and also display split transient absorption bands; whereas PDI dimers with smaller PDI-PDI torsional angles and flexible structures display weaker UV-Vis and CD exciton coupling and a single transient absorption band. The excimer fluorescence maxima and decay times for all of these DNA-PDI constructs are similar.

Introduction

Perylenediimide (PDI) and its derivatives have an unusual propensity to form self-assembled dimers and higher aggregates and thus have been incorporated into a variety of supramolecular structures.[1-4] The PDI chromophore has several advantages in studies of self-association including structured absorption spectra which display characteristic changes upon dimer or aggregate formation and high thermal and photochemical stability. The structure and electronic spectroscopy of the simplest of aggregates, the PDI dimer, have been the subject of numerous experimental and theoretical investigations. Several quantum mechanical studies of the unconstrained gas phase PDI dimer have shown that it adopts a co-facial geometry with a torsional angle of *ca*. 30° between the PDI long axes.[5-8] The ground state geometry is expected to determine the extent of exciton coupling and hence the appearance of the UV-Vis absorption and circular dichroism (CD) spectrum.[9, 10] However, relaxation of the excited state dimer geometry could lead to time-dependent changes in the appearance of the fluorescence and transient absorption spectra of the excited PDI dimers.[11] Such changes should be more pronounced in dimers with flexible *vs*. rigid ground state geometries.

We have reported the synthesis and selected properties of several bis(oligonucleotide) conjugates possessing the PDI linker $\mathbf{P_L}$ which form PDI dimers upon association (Chart 1a). These include complementary single strand conjugates such as **G** and **C** which form the duplex **G:C** upon hybridization,[12] the PDI-linked hairpin **H8** which forms the hairpin dimer $(\mathbf{H8})_2$,[13] and dumbbells having two PDI linkers which form 1-dimensional polymers upon PDI association.[14] We have also reported the synthesis and selected properties of several hairpin-forming conjugates that incorporated two or more adjacent PDI base surrogate $\mathbf{P_S}$ (Chart 1b).[15] These include the hairpins **2AT** and **2AA**. All of the conjugates in Chart 1 that contain two PDI chromophores display similar "dimer-like" UV-Vis spectra, namely $A^{0\text{-}0}/A^{0\text{-}1}$ vibronic band intensity ratios which are distinctly smaller than the values for PDI monomers due to exciton coupling.[6, 16-18] However, the sign and intensity of their CD spectra are strongly dependent upon their ground state geometries. For example, the duplex **G:C** displays a strong exciton coupled CD spectrum in the wavelength region of the PDI long-wavelength absorption band; whereas, the hairpin dimer $(\mathbf{H8})_2$ displays only a weak CD spectrum.[12, 13] As

shown in Fig. 1, the structures obtained for both **G:C** and $(\mathbf{H8})_2$ from molecular dynamics simulations have π-stacked geometries; however, the former has a more rigid geometry with a dihedral angle of 38° between the PDI long axes; whereas the latter has a low inter-hairpin torsional barrier with minima near ±20°.[12]

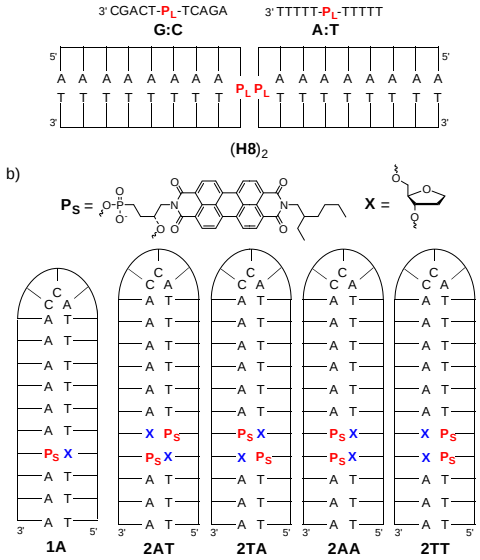

Chart 1. (a) Structures of the PDI linker $\mathbf{P_L}$, the duplexes **G:C** and **A:T** and the hairpin dimer $(\mathbf{H8})_2$ and (b) the PDI base pair surrogate $\mathbf{P_S}$ and abasic site **X** and hairpins containing $\mathbf{P_S}$.

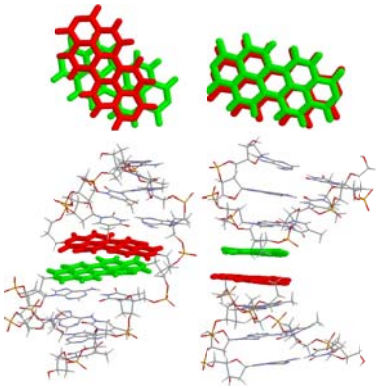

Fig. 1. Average orientation of the two PDI residues in duplex **G:C** (left) and hairpin dimer $(\mathbf{H8})_2$ (right, see Chart 1a for structures) viewed from top and side (only three base pairs on each side of the hairpin dimer are shown).

In spite of the numerous investigations of PDI-DNA conjugates,[3] there have been no systematic studies of the relationship between their ground state structures and UV-Vis, CD, or fluorescence spectra. In addition, their excited state transient absorption spectra remain largely unexplored, aside from our studies of the hairpin dimer $(\mathbf{H8})_2$.[13, 19] We report here the results of a collaborative investigation of the ground state structures and the steady state and time-resolved spectra of the four isomeric hairpins **2AT**, **2TA**, **2AA**, and **2TT**, which possess the PDI base surrogate $\mathbf{P_S}$ either in the same or opposite strands and for the duplex **A:T**, an analogue of duplex **G:C** (Chart 1a), which possesses only A-T base pairs. The results for these hairpins are compared with our published results for the hairpin dimer $(\mathbf{H8})_2$. Differences in ground state PDI dimer conformation for these six DNA-PDI conjugates, as derived from molecular dynamics simulations, are related to differences in both ground and excited state electronic spectra.

Results and Discussion

Synthesis and Molecular Modelling

The conjugates shown in Chart 1a were prepared as previously described,[12, 13, 19] using the procedure of Rahe, *et al*.[20] for incorporation of the linker $\mathbf{P_L}$. The hairpins shown in Chart 1b were prepared as previously reported,[15, 21] following the procedure of Wagner and Wagenknecht for preparation of the base surrogate $\mathbf{P_S}$.[22] All conjugates were purified and characterized as described in the Experimental Section.

Quantum mechanical studies of the unconstrained gas phase PDI dimer have shown that it adopts a co-facial geometry with a relatively flat potential energy surface having global minimum with zero displacement of molecular centers.[5-8] A minimized torsional angle of *ca*. 30° between PDI long axes is attributed to attractive electronic interactions between the imide carbonyl and nitrogen groups. In view of the flat potential energy surface, the geometry of PDI dimer in a DNA conjugate structure might be expected to be influenced by the local DNA structure as well as the PDI-PDI interactions. In the absence of NMR or X-ray structures for DNA-PDI conjugates, we have relied upon molecular dynamics simulations to obtain minimized structures for a wide range of DNA systems including DNA-PDI conjugates.[12, 23, 24] We previously reported the minimized structures for the duplex **G:C** and the hairpin dimer $(\mathbf{H8})_2$ (Chart 1), both of which have co-facial PDI dimer structures.[12] As shown in Fig. 1, the former has a slipped geometry with a twist angle of 38° between PDI long axes; whereas, the latter has either a parallel or antiparallel eclipsed PDI-PDI geometry with twist angles *ca*. ± 20°, somewhat smaller than for the gas phase PDI dimer.

In the present study we have employed molecular dynamics simulations to investigate the PDI dimer structure for the three hairpin conjugates **2AT**, **2TA**, and **2TT** (Fig. 2). Replacing two adjacent A-T base pairs in canonical B-DNA with a $\mathbf{P_S}$ base surrogate opposite a tetrahydrofuran abasic site analogue (**X**, Chart 1b) might be expected to yield antiparallel PDI chromophores when the two PDI's are located in opposite strands and parallel chromophores when the PDI's are located in the same strand. The minimized structures for **2TA** and **2TT** are consistent with this expectation and have average PDI-PDI torsion angles of *ca*. 160° and 20°, respectively (Fig. 3), similar to those for the unconstrained hairpin dimer $(\mathbf{H8})_2$, and approximately Gaussian probability distributions. However, **2AT** has a parallel dimer structure with a probability distribution that has a maximum value near 50°. Inspection of the minimized structure for **2AT** (Fig. 2) shows that the two

bulky *N*-alkyl substituents cannot readily rotate past each other and thus fix the PDI-PDI dihedral angle at a relatively large positive value. No such barrier to rotation is apparent in the structures of **2TA** or **2TT**. As will become evident, this difference in minimized ground state geometry provides the basis for understanding the pronounced differences in the ground and excited state electronic spectra of the PDI dimers.

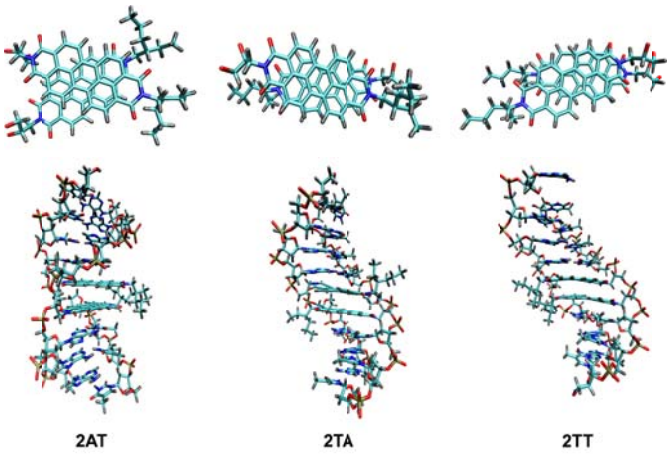

Fig. 2. (Top) Overlap between the PDI chromophores and (bottom) the average structures of hairpins **2AT**, **2TA** and **2TT** from 6 ns MD simulations (only three base pairs on either side of PDI dimer are shown). See Chart 1b for hairpin structures.

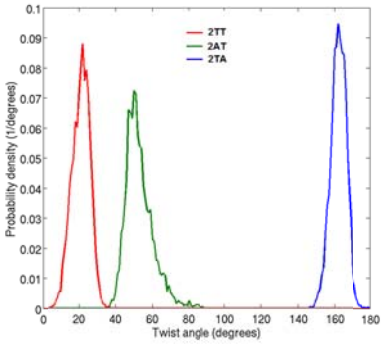

Fig. 3. Probability distributions for the twist angles between the two PDI residues in hairpins **2AT**, **2TA** and **2TT**.

UV-Vis Spectra

The long wavelength region of the UV-Vis spectrum of the diol derivative of chromophore $\mathbf{P_S}$ ($\mathbf{P_S(OH)}$, Chart S1, ESI) has a A^{0-0}/A^{0-1} band intensity ratio of *ca*. 1.66, slightly larger than the value for the hairpin **1A**, and characteristic of PDI monomers.[11] The UV-Vis spectra of the hairpins **2AT**, **2TA**, **2AA**, and **2TT** in aqueous buffer (Fig. 4a) have inverted band intensity ratios (A^{0-0}/A^{0-1} = < 1.0, Table 1). The smaller band intensity ratios for the PDI dimers *vs*. monomer are attributed to exciton coupling between the co-facial PDI chromophores in the dimers.[7, 11] The band intensity ratios for the *anti* isomers **2AT** and **2TA** are lower than those for the *syn* isomers **2TT** and **2AA** (Table 1) and the PDI bands for *syn* isomer are noticeably broader than those for the *anti* isomers (Fig. 4a).

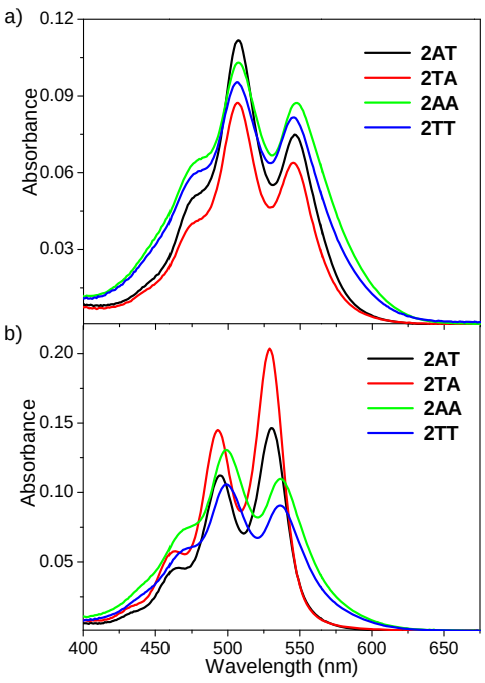

Fig. 4. UV-Vis spectra of hairpins **2AT**, **2TA**, **2AA** and **2TT** a) in buffer and b) in DMSO. Concentrations were adjusted to provide an absorbance of *ca*. 0.1 at the A^{0-1} band of PDI.

The UV-Vis spectra of the duplex **A:T** and hairpin dimer $(\mathbf{H8})_2$ also have inverted PDI band intensity ratios (A^{0-0}/A^{0-1} = 0.66 and 0.60, respectively) when compared to that for the diol derivative of $\mathbf{P_L}$ ($\mathbf{P_L(OH)}$, Chart S1, ESI).[12, 13] Thus both the A^{0-0}/A^{0-1} ratio and the extent of band broadening are dependent upon the ground state structure of the dimer, as observed in previous studies.[25, 26]

The long-wavelength regions of the UV-Vis spectra of **2AA** and **2TT** are largely unchanged in the polar aprotic solvent DMSO *vs*. aqueous buffer; whereas the spectra of **2AT** and **2TA** in DMSO resemble those of the PDI monomer in **1A** (Fig. 4b). Bonner and Klibinov have reported that a 21-mer DNA duplex is completely dissociated in DMSO.[27] Thus we expected that hairpin base pair dissociation would occur in DMSO. The values of A^{0-0}/A^{0-1} for **2AT** and **2TA** are, in fact, larger at room temperature in DMSO (1.30 and 1.40, respectively) than in aqueous buffer; however they are smaller than the values of 1.5-1.6 expected for isolated PDI chromophores in DNA. Evidently the PDI chromophores of **2AT** and **2TA** are largely but not completely dissociated in DMSO; whereas, the chromophores of **2AA** and **2TT** remain associated.

The 260 nm absorbances for the hairpins **2AT**, **2TA**, **2AA**, and **2TT** increase continuously upon heating (Fig. S1a, ESI). The absence of a well-defined melting transition is attributed to the lack of cooperative melting for the two hairpin A-T base pair domains (loop and stem regions) and the PDI-PDI hydrophobic stacking interaction. The A^{0-0}/A^{0-1} ratios for these hairpins also increase continuously upon heating (Fig. S1b, ESI). The maximum values of A^{0-0}/A^{0-1} at 95 °C are *ca*. 0.85

Table 1. UV-Vis and steady state fluorescence data of PDI-DNA conjugates in aqueous buffer and DMSO.[a]

conjugate (solvent)		absorption		fluorescence			
		A^{0-0}, A^{0-1} (nm)[b]	A^{0-1}/A^{0-0} [c]	λ_M (nm)[d]	λ_E (nm)[e]	$\Phi_{Total,\%}$ [f]	%E[g]
(H8)$_2$ (buffer)		545, 505	0.60	553	657	0.083	33
A:T (buffer)		547, 507	0.66	552	665	0.96	100
1A (buffer)		547, 508	1.53			< 0.1	0
2AT	buffer	546, 507	0.69	550, 596	650	0.41	44
	DMSO	530, 495	1.30[f]	539, 580	640		0
2TA	buffer	546, 507	0.73	550, 600	649	0.26	65
	DMSO	529, 493	1.40[f]	538, 579	635		0
2AA	buffer	547, 507	0.85	550	655	0.25	100
	DMSO	537, 499	0.84[f]	540	655		100
2TT	buffer	545, 506	0.84	549	656	0.33	92
	DMSO	536, 499	0.86[f]	540	654		100

[a] Concentrations of conjugates adjusted to provide an absorbance of *ca*. 0.1 at the PDI long-wavelength absorption maximum. All spectra recorded at room temperature. [b] UV-Vis absorption maxima corresponding to the two long wavelength absorption maxima of the PDI chromophore. [c] Ratio of band intensities. [d] Fluorescence maxima assigned to the PDI monomer. [e] Fluorescence maxima assigned to the PDI excimer. [f] Sum of monomer and excimer fluorescence. [g] % of room temperature emission assigned to the excimer.

for **2AT** and **2AA** and 1.0 for **2TA**. These values are significantly lower than the value of 1.5-1.6 for isolated PDI chromophores, indicative of substantial PDI-PDI hydrophobic association well above the base-pair melting temperature, even when the PDI chromophores are separated by 16 nucleotides in the disordered structures of **2AT** and **2TA**. This result is consistent with the observation by Wang *et al*. of increased association at high temperatures for PDI chromophores separated by an 18-mer mixed base single strand which was attributed to thermophilic π-stacking of the PDI chromophores.[28]

Circular Dichroism Spectra

The CD spectra of hairpins **2AT**, **2TA**, **2AA**, and **2TT** and the duplex **A:T** display short-wavelength maxima and minima characteristic of B-DNA duplexes (Fig. 5, S2 and S3, ESI), as previously reported for the duplex **G:C** and hairpin dimer **(H8)$_2$**.[12] The long-wavelength region of the CD spectra for the hairpins consists of a positive band at longer wavelength and a negative band at shorter wavelength (positive Cotton effect) of approximately equal intensity, corresponding to the two exciton bands of the dimer absorption spectrum (Fig. S2, ESI). The spectrum of **2AT** is the most intense of these, consistent with the larger twist angle between the two PDI chromophores (Fig. 3) and its more rigid structure, as indicated by the MD simulations (Fig. 2).

The long wavelength region of the CD spectrum of **A:T** (Fig. S3, ESI) is similar to that reported for **G:C**, consisting of a negative band at longer wavelength and a positive band of approximately equal intensity at shorter wavelength (negative Cotton effect).[12] A positive Cotton effect might have been expected for a pair of chromophores imbedded in a right-handed B-DNA duplex, as previously observed for a similar duplex having stilbenedicarboxamide linkers.[29, 30] The spectrum of hairpin **(H8)$_2$** (Fig. S3, ESI) displays a weak negative band at long wavelengths with vibronic maxima similar to that of the absorption spectrum of **P_L(OH)** and is assigned to induced circular dichroism of the achiral chromophore in a chiral environment.[13] The absence of a conservative dimer CD spectrum was attributed to the presence of nearly equal amounts of dimers having positive and negative dihedral angles between their long axes. However, as noted by Cantor and Schimmel, the intensity of the CD spectrum of a dimer may vanish for many conformations of the dimer, including those with coplanar chromophores.[31]

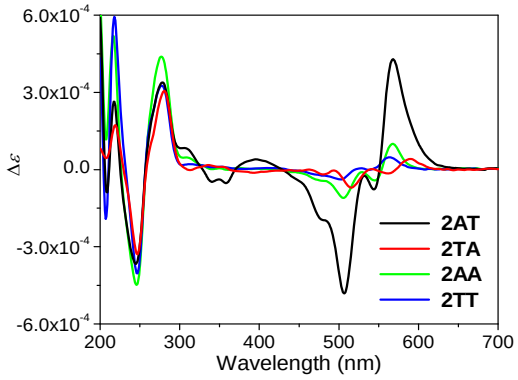

Fig. 5. Circular dichroism spectra of hairpins **2AT**, **2TA**, **2AA** and **2TT** in buffer. Concentrations were adjusted so as to have an absorbance *ca*. 0.1 at the A^{0-1} band of PDI.

The intensity of both positive and negative CD bands for the hairpin **2AT** decrease upon heating and the sign of the Cotton effect undergoes inversion from positive to negative above 90 °C (Fig. S4, ESI). The first derivative of a plot of CD intensity *vs*. temperature has a broad maximum at *ca*. 75 °C, approximately 5 °C higher than the T_M value for **2AT** determined from UV-Vis data (Fig. S1, ESI). The similar shape of the CD spectrum of **2AT** at low and high temperatures provides further evidence for the absence of complete thermal dissociation of the PDI dimer even at high temperatures. As previously reported, CD melting temperatures obtained from

the temperature-dependence of the CD spectra of **G:C** and $(\mathbf{H8})_2$ are similar to those obtained from UV-Vis melting profiles.[12]

Fluorescence Spectra and Decay Times

The fluorescence quantum yields for hairpins **1A**, **2AT**, **2TA**, **2AA**, and **2TT** in aqueous buffer are very low (< 5 x 10^{-3}, Table 1), consistent with quenching of PDI monomer fluorescence by adenine[21] and, to a lesser extent, the forbidden nature of PDI excimer fluorescence.[11, 32] The spectra of **2AA** and **2TT** are dominated by excimer fluorescence whereas the spectra of **2AT** and **2TA** have comparable amounts of monomer and excimer emission (Fig. 6a). The fluorescence excitation spectra of the structured monomer emission of **2AT** and **2TA** resemble that of the PDI monomer; whereas the excitation spectra of **2AA** and **2TT** resemble that of the PDI dimer (Fig. S5, ESI). Thus the monomer emission from **2AT** and **2TA** can be attributed, at least in part, to hairpin conformations in which there is poor π-overlap between the $\mathbf{P_S}$ chromophores in opposite strands. Conversely, the absence of monomer emission from **2AA** and **2TT** suggests that the populations of poorly-stacked intra-strand conformations are very small for these hairpins.

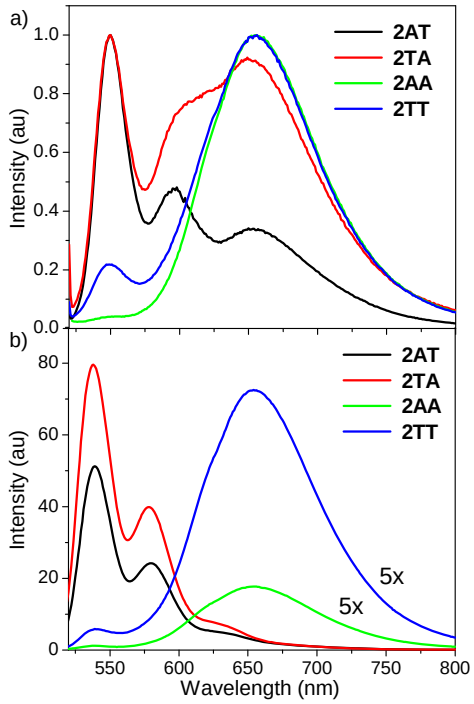

Fig. 6. Fluorescence spectra of hairpins **2AT**, **2TA**, **2AA** and **2TT** in a) buffer and b) DMSO. Concentrations of oligonucleotides were adjusted to provide an absorbance *ca*. 0.1 at the $A^{0\text{-}1}$ band of PDI. Excitation wavelength, 505 nm.

The fluorescence of the hairpin dimer $(\mathbf{H8})_2$ (Chart 1a) which possesses the PDI chromophore $\mathbf{P_L}$ has a low excimer/monomer ratio in buffer with 100 mM NaCl; monomer emission being attributed to the presence of hairpin monomer **H8** in equilibrium with the dimer under these conditions. Increasing salt concentration or decreasing temperature results in a decrease in monomer concentration and an increase in the ratio of excimer/monomer fluorescence intensity.[13] The spectrum of the duplex **A:T** resembles that of **2AA** and is dominated by excimer emission, consistent with the minimized geometry of duplex **G:C** in which a π-stacked structure is enforced by the duplex geometry (Fig. 1).

Table 2. Decay times for fluorescence and transient absorption. [a,b]

Conjugate	Fluorescence decay		Transient absorption decay[e]	A_{625}/A_{707} rise[f]
	τ_m, ns [c]	τ_e, ns [d]	τ_d, ns	τ_r, ps
$\mathbf{P_L(OH)}$	3.9		4.1	
$(\mathbf{H8})_2$	0.28 (37%) 1.7 (64%)	τ_1 = 0.14 (14%) τ_2 = 1.5 (86%)	1.3 ± 0.1	22
A:T	[g]	τ_1 = 0.16 (17%) τ_2 = 1.8 (83%)	1.4 ± 0.1	6.5
$\mathbf{P_S(OH)}$	2.7		0.098 (18%) 2.3 (82%)	
1A	0.032		0.036	
2AT	τ_1 = 0.49 (57%) τ_2 = 2.1 (43%)	τ_1 = 0.35 (24%) τ_2 = 2.5 (76%)	2.3 ± 0.1	9.4
2TA	τ_1 = 0.027 (90%) τ_2 = 0.74 (7%) τ_3 = 2.5 (3%)	τ_1 = 0.31 (36%) τ_2 = 2.2 (64%)		
2AA	[g]	τ_1 = 0.29 (23%) τ_2 = 1.2 (77%)	0.73 ± 0.05	33
2TT	[g]	τ_1 = 0.81 (56%) τ_2 = 1.83 (43%)		

[a] Concentrations of conjugates adjusted to provide an absorbance of *ca*. 0.1 at the PDI long-wavelength absorption maximum. All data obtained at room temperature. [b] Values in parentheses are amplitudes of decay components. [c] Monomer decay determined at 560 nm. [d] Excimer decay determined at 660 nm. [e] Decay of transient absorption determined at *ca*. 700 nm. Similar single wavelength decays determined at other wavelengths. [f] Rise time for the ratio of 625nm/707nm transient absorbance intensity. [g] Very weak monomer fluorescence.

The fluorescence decay times of hairpins **2AT**, **2TA**, **2AA**, and **2TT** (Fig. S6, ESI) and duplex **A:T** determined at the wavelengths corresponding to the maximum intensity of monomer and excimer fluorescence are reported in Table 2, along with the decay times for the diol derivatives ($\mathbf{P_L(OH)}$ and $\mathbf{P_S(OH)}$), hairpin dimer $(\mathbf{H8})_2$ and hairpin **1A**.[13, 21] The decay times for $\mathbf{P_L(OH)}$ and $\mathbf{P_S(OH)}$ are somewhat shorter than that for an *N*,*N*'-dialkyl-PDI derivative studied by Giaimo *et al*. (τ = 4.5 ns);[11] whereas the decay time for **1A** is significantly shorter.[21] The short decay time of **1A**, like its low fluorescence quantum yield, is attributed to electron transfer quenching by neighbouring adenine bases. The lower energy excimers are less sensitive to electron transfer quenching by adenine.[19]

The monomer decays for the PDI dimer hairpins are best fit as multiple exponentials, with the longest decay time similar to that of $\mathbf{P_S(OH)}$. The shortest monomer decay time for **2TA** is similar to that for **1A** and can be tentatively assigned to poorly-stacked conformations of the PDI chromophores within the base-paired hairpin. The 660 nm excimer fluorescence decays are best fit as dual exponentials. The average excimer fluorescence decay times for all of the PDI dimers are similar

(0.94-1.6 ns). The excimer decay times for **2AT** and **2TA** are similar to those for the 560 nm monomer fluorescence decays suggesting that at least part of the monomer fluorescence may arise from dissociation of the excimer. Excimer dissociation to form the fluorescent monomer was observed by Li *et al*. for single strand PDI-DNA foldamers.[18] In view of the low values of Φ_{fl} for all of our PDI-DNA conjugates (Table 1), singlet decay must occur predominantly *via* non-radiative pathways. The time-resolved emission spectra for **2AT** and **2TA** (Fig. S7, ESI) have a higher ratio of excimer/monomer fluorescence at long *vs*. short delay times (2.0 or 1.4 ns *vs*. 0.25 or 0.20 ns, respectively), in accord with the longer delay time for excimer *vs*. monomer fluorescence decay (Table 2). Monomer emission from **2AA** and **2TT** is very weak at both short and long delay times.

The fluorescence spectra of the *anti* hairpins **2AT** and **2TA** in DMSO are dominated by monomer emission (Fig. 6b); however, the fluorescence spectra of the *syn* hairpins **2AA** and **2TT** are similar in DMSO and buffer, being dominated by excimer emission in both solvents. The effect of the polar aprotic solvent DMSO on the fluorescence spectra of these hairpins is consistent with its effect upon their absorption spectra (Fig. 4b). Evidently, base pair denaturation by DMSO separates the interstrand PDI dimers but leaves the intrastrand dimers largely intact. Thermal denaturation has an effect similar to that of DMSO upon the fluorescence spectra of the hairpin PDI dimers (Fig. 7 and S8, ESI). Upon heating from 5 to 95 °C, the ratio of monomer/excimer fluorescence intensity for **2AT** and **2TA** continuously increases.

Transient Absorption Spectra

The transient absorption spectra of the hairpin **1A** have previously been reported and are reproduced in Fig. S9, ESI. It displays negative bands with maxima at 507, 550, and 605 nm and a single positive band with a maximum at 705 nm. The 507 and 605 nm bands are assigned to ground state depopulation and stimulated emission, respectively, of the $\mathbf{P_S}$ chromophore, while the negative band at 550 nm is assigned to the overlapping 0,0 bands of ground state absorption and stimulated emission. The 705 nm band is assigned to the overlapping absorption bands of $^{1*}\mathbf{P_S}$ and $\mathbf{P_S}^{-\cdot}$, which is formed upon photooxidation of adenine by $^{1*}\mathbf{P_S}$. The decay time of the 705 nm band of **1A** is essentially the same as that of its fluorescence decay (Table 2), indicating that $^{1*}\mathbf{P_S}$ is formed upon charge recombination of the $\mathbf{P_S}^{-\cdot}$-$A^{+\cdot}$ charge-separated state.[21]

The transient spectra of hairpin dimer $(\mathbf{H8})_2$, duplex **A:T**, and hairpins **2AT** and **2AA** (Fig. 8) all display negative bands with minima near 505 and 550 nm and broad positive bands at longer wavelength. The decay times of all of these bands can be fit as single exponentials having decay times that are independent of wavelength (Table 2). The negative bands have band intensity ratios similar to that of the UV-Vis absorption spectra and are assigned to the ground state bleach of the PDI dimer absorption. The absence of a 605 nm negative band could reflect either the absence of stimulated emission or overlap between weak stimulated emission and a strong absorption band in the same wavelength region. At short delay times the positive bands have maxima between 605-625 nm and a second maxima or shoulder between 705-725 nm. The most pronounced band splitting is observed for duplex **A:T** (Fig. 8d). We previously reported that the transient absorption spectrum of dimer $(\mathbf{H8})_2$ undergoes a time-dependent change in band shape to a single maximum at 650 nm (Fig. 8a),[13] similar to that for the co-facial PDI dimer studied by Giaimo *et al*.[11] This change was attributed to geometric relaxation of the excimer-like $^{1*X}\mathbf{PDI_2}$ Frank-Condon state which has an angle of *ca*. 20° between PDI electronic transition dipoles to a relaxed state having an angle of *ca*. 0° (Fig. 9).

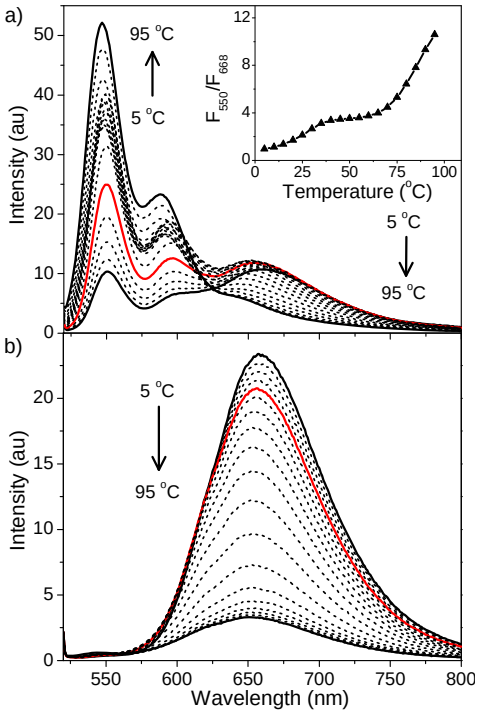

Fig. 7. Fluorescence spectra of (a) **2AT** and (b) **2AA** as a function of temperature in buffer. Red traces indicate the fluorescence spectra at 25 °C. Inset of (a) shows the ratio of the fluorescence intensity at 550 to 668 nm (F_m/F_{ex}) *vs*. temperature. Excitation wavelength, 505 nm.

A similar, but less pronounced time-dependent change in band shape is observed for the positive band of hairpin **2AA** (Fig. 8c). Minor changes in band shape are observed for hairpin **2AT** and duplex **A:T** at short delay times (Fig. 8b,d), but no changes are observed at longer times. Global analysis of the transient absorption of $(\mathbf{H8})_2$ shows that band narrowing occurs with a time constant of 14 ps.[13] Band-narrowing times obtained from plots of the time-dependence of the ratio of 625/708 nm band intensities are reported in Table 2. The value for $(\mathbf{H8})_2$ (22 ps) is slightly longer than that obtained from global analysis. The value for **2AA** is still-longer (33 ps); whereas values for **A:T** and **2AT** are significantly shorter (< 10 ps).

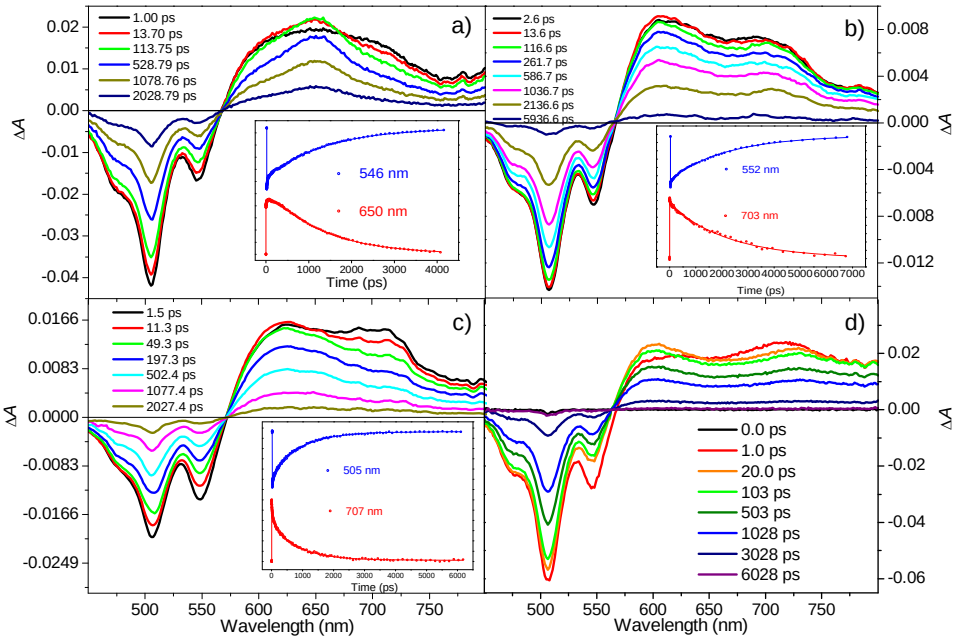

Fig. 8. Transient absorption spectra of hairpins (a) $(\mathbf{H8})_2$, (b) **2AT**, (c) **2AA**, and (d) **A:T** in buffer following excitation with 505 nm, 120 fs laser pulses. Insets show transient absorption kinetics at specified wavelengths. Nonlinear least-squares fits to the data are also shown.

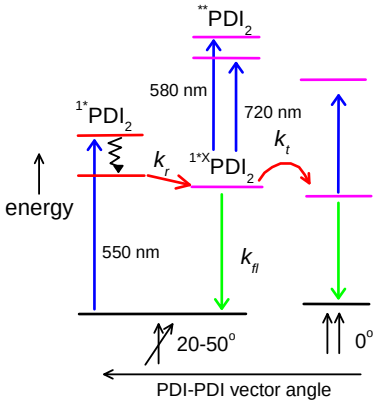

Fig. 9. Energy level diagram for PDI dimer excited states. Vertical blue arrows indicate ground and excited state absorption, red arrows geometric relaxation, and green arrows excimer fluorescence.

The short band-narrowing times and minor changes in band shape for the latter systems are suggestive of very minor changes in PDI dimer geometry following electronic excitation. Band-narrowing for **2AA**, like that for $(\mathbf{H8})_2$, can be attributed to geometric relaxation in the excited state (Fig. 9). The MD simulation for **2AA** shows a shallow potential with a minimum near 20° for the $\mathbf{P_S}$ dimer in **2AA**. A slightly higher barrier for excited state geometric relaxation toward 0° could account for the slower relaxation time for **2AA** *vs*. $(\mathbf{H8})_2$. The minimized ground state torsion angles for **G:C** and **2AT** are much larger, 38° and 50° respectively, than that for **2AA** and presumably both systems have larger barriers for excited state relaxation toward 0°. The relatively fast low amplitude rise of the A_{625}/A_{707} band intensity ratio for these systems may reflect vibrational cooling of the excited dimer.

The similar fluorescence and transient absorption decay times for **A:T** and **2AA** suggests that the two absorption bands arise from two transitions from a single excited state, rather than transitions from two different excited states. Whereas $(\mathbf{H8})_2$ and **2AA** and other PDI dimers have non-eclipsed ground state geometries, low barriers to excited state torsion permit them to undergo geometric relaxation in competition with excimer decay, in which case a single transient absorption band is observed at longer delay times. Thus, the appearance of the transient absorption spectrum of the PDI-DNA conjugate dimers is dependent upon the presence or absence of a barrier between the Frank-Condon excited state and the relaxed eclipsed excimer geometry, as shown schematically in Fig. 9.

Concluding Remarks

The effects of formation of co-facial PDI dimers upon the ground and excited state electronic spectra of six DNA-PDI conjugates have been investigated and correlated with the structures of the ground state dimers which were determined by molecular dynamics simulations. The UV-Vis spectra of all the conjugates display broadening of the PDI absorption band and inversion of the relative intensities of the $A^{0\text{-}0}$ and $A^{0\text{-}1}$ bands when compared to those of the PDI monomers. These changes are attributed to exciton coupling between the adjacent PDI chromophores. Small $A^{0\text{-}0}/A^{0\text{-}1}$ band intensity ratios and strong CD exciton coupling are observed for the duplex **A:T** and hairpin **2AT** which possess relatively large PDI-PDI dihedral angles. The CD spectra of these conjugates have opposite signs, indicative of a difference in the chirality of their chromophore environments. The hairpin dimer $(\mathbf{H8})_2$ displays the smallest $A^{0\text{-}}$

$^0/A^{0-1}$ band intensity ratio but does not display exciton-coupled CD. This seemingly anomalous behaviour may reflect the presence of comparable amounts of *syn* and *anti* hairpin dimers.[13]

All of the dimers display excimer fluorescence accompanied by variable amounts of monomer fluorescence (0-65%, Table 1). The intrastrand dimers **2AA** and **2TT** and the duplex **A:T** show little or no monomer emission whereas the interstrand dimers **2AT** and **2TA** and the hairpin dimer $(\mathbf{H8})_2$ show large amounts of monomer emission. Excitation spectra indicate that monomer fluorescence can be attributed to ground state conformations with monomer-like absorption spectra. All of the dimers have similar excimer fluorescence maxima and dual exponential fluorescence decays with similar short- and long-lived components (Tables 1 and 2). Thus the properties of the fluorescent excimers appear to be independent of ground state geometry.

The transient absorption spectra of all four dimers that we have investigated initially display two transient absorption bands (Fig. 8). Dimers **A:T** and **2AT** which have relatively rigid structures, as judged by their strong CD spectra as well as molecular dynamics simulations, undergo little change in band shape during the transient decay process. However, dimers $(\mathbf{H8})_2$ and **2AA** which have flexible structures undergo band narrowing with time constants of 22 ps and 33 ps (Table 2), respectively, attributed to the changes in the torsion angles between PDI chromophores (Fig. 9). Thus transient absorption band splitting may prove diagnostic of rigid structures with relatively large dihedral angles between PDI transition dipoles.

In summary, this investigation has revealed that the spectroscopic properties of the ground and excited states of co-facial PDI dimers embedded in DNA constructs display pronounced dependence upon the geometry imposed by the construct in aqueous buffer and in the denaturing solvent DMSO.

Experimental Section

Materials. PDI derivatives $\mathbf{P_L}$ and $\mathbf{P_S}$ were synthesized as per the reported procedures.[20, 22] PDI-oligonucleotide conjugates were prepared by means of conventional phosphoramidite chemistry using an Expedite DNA synthesizer following the procedure of Letsinger and Wu.[29] All of the 2'-deoxynucleotide phosphoramidites, DNA synthesizing reagents, and controlled pore glass solid supports (CPG) were purchased from Glen Research (Sterling, VA). Following synthesis, the conjugates were first isolated as trityl-on derivatives by reverse-phase (RP) HPLC, then detritylated in 80% acetic acid for 30 min, and re-purified by RP-HPLC as needed. RP-HPLC analysis was carried out on a Dionex chromatograph. Molecular weights of representative conjugates were determined by means of MALDI-TOF mass spectroscopy with a Bruker Autoflex spectrometer.

Computational Methods: Computational details for **G:C** and $(\mathbf{H8})_2$ have been reported.[12] For modelling **2AT**, **2TA** and **2TT**, two PDI containing species were simulated using the Amber99 force field.[33] Starting structures for the DNA segment were taken to be B-DNA and the PDI residues were added manually. The systems were then minimized and simulated in a TIP3P solvent box with an 8.0 Å buffer. All simulations were carried out using the Amber10 program with particle mesh Ewald treatment of the long range electrostatics.[34] Following minimization, a 2 ns equilibration run was performed followed by a 6 ns production run. All MD simulations were performed at 300 K and 1 bar of pressure using the NPT ensemble.

Electronic Spectroscopy. Unless otherwise noted, all the spectroscopic measurements were done in 10 mM phosphate buffer (pH 7.2) containing 0.1 M NaCl using freshly prepared sample solution. As the molar absorption coefficients of aggregated PDI's are unknown, the accurate determination of the concentration of oligonucleotides containing multiple PDI's was not possible. Therefore, for spectral measurements the absorbance of all the samples was normalized at the A^{0-1} band of PDI chromophore irrespective of the total oligonucleotide concentration. UV-Vis spectra and thermal dissociation profiles were measured on a Perkin-Elmer Lambda 2 spectrophotometer equipped with a Peltier sample holder and a temperature programmer for automatically increasing the temperature at the rate of 0.5 °C/min. Circular dichroism spectra were obtained using a JASCO J-815 spectropolarimeter equipped with a Peltier sample holder and temperature controller. Temperature was increased at a rate of 0.5 °C/min. Fluorescence spectra were obtained using a Spex Fluoromax spectrofluorimeter. Fluorescence quantum yields were determined using 470 nm excitation by comparing the integrated fluorescence area with that for fluorescein in 0.1 M NaOH.

Fluorescence Lifetimes. Fluorescence lifetime measurements were performed using a frequency-doubled, cavity-dumped Ti:sapphire laser as the excitation source and a Hamamatsu C4780 ps fluorescence lifetime measurement system, as described previously.[35] The energy of the 400 nm, 25 fs pulses was attenuated to ~1.0 nJ/pulse in all of the fluorescence lifetime experiments. The total IRF of the streak camera system was 20 ps. Data were collected for each sample at the same concentrations as for the steady-state data. All of the fluorescence data were acquired in single-photon counting mode using the Hamamatsu HPD-TA software. The data was fit using the Hamamatsu fitting module and deconvoluted using the laser-pulse profile.

Transient Absorption Spectroscopy. Femtosecond measurements were made using a Ti:sapphire laser system as previously described.[36] The instrument response function (IRF) for the pump-probe experiments was 180 fs. Typically, 5 s of averaging was used to obtain the transient spectrum at a given delay time. Solutions of conjugates in TE buffer and 0.1 M NaCl were prepared in cuvettes having a 2 mm path length and irradiated with 505 nm, 130 fs, 0.1-1.0 μJ pulses focused to a spot with a diameter of 200 μm. The optical density at λ_{ex} was between 0.2-0.4. Laser scatter at 505 nm was subtracted from the transient spectra. Analysis of the kinetic data was performed at multiple wavelengths using a Levenberg-Marquardt nonlinear least-squares fit to a general sum-of-exponentials

function with an added Gaussian to account for the finite instrument response.

Acknowledgements

This work supported by grants from the National Science Foundation, Collaborative Research in Chemistry (CHE-0628230 to FDL and MRW) and the Chemical Sciences, Geosciences, and Biosciences Division, Office of Basic Energy Sciences, DOE under grant number DE-FG02-99ER14999 (MRW).

Notes and references

[*]Department of Chemistry and Argonne-Northwestern Solar Energy Research (ANSER) Center, Northwestern University, Evanston, IL 60208-3113. E-mail: fdl@northwestern.edu

†Electronic Supplementary Information (ESI) available: UV-Vis, circular dichroism, fluorescence, and transient absorption spectra (Fig. S1-S9). See DOI: 10.1039/b000000x/

1. F. Wurthner, *Chem. Commun.*, 2004, 1564-1579.
2. T. Weil, T. Vosch, J. Hofkens, K. Peneva and K. Müllen, *Angew. Chem. Int. Ed.*, 2010, **49**, 9068-9093.
3. D. Görl, X. Zhang and F. Würthner, *Angew. Chem. Int. Ed.*, 2012, **51**, 6328-6348.
4. A. D. Q. Li, in *Molecular Self-Assembly*, ed. A. D. Q. Li, Pan Stanford Publishing, 2012, pp. 123-206.
5. A. E. Clark, C. Qin and A. D. Q. Li, *J. Am. Chem. Soc.*, 2007, **129**, 7586-7595.
6. J. Seibt, P. Marquetand, V. Engel, Z. Chen, V. Dehm and F. Wurthner, *Chem. Phys.*, 2006, **328**, 354-362.
7. R. F. Fink, J. Seibt, V. Engel, M. Renz, M. Kaupp, S. Lochbrunner, H.-M. Zhao, J. Pfister, F. Würthner and B. Engels, *J. Am. Chem. Soc.*, 2008, **130**, 12858-12859.
8. H.-M. Zhao, J. Pfister, V. Settels, M. Renz, M. Kaupp, V. C. Dehm, F. Würthner, R. F. Fink and B. Engels, *J. Am. Chem. Soc.*, 2009, **131**, 15660-15668.
9. M. Kasha, H. R. Rawls and M. A. El-Bayoumi, *Pure Appl. Chem.*, 1965, **11**, 371-392.
10. N. Harada and K. Nakanishi, *Circular Dichroic Spectroscopy. Exciton Coupling in Organic Stereochemistry*, University Science Books, Mill Valley, CA, 1983.
11. J. M. Giaimo, J. V. Lockard, L. E. Sinks, A. M. Scott, T. M. Wilson and M. R. Wasielewski, *J. Phys. Chem. A*, 2008, **112**, 2322-2330.
12. Y. Zheng, H. Long, G. C. Schatz and F. D. Lewis, *Chem. Commun.*, 2005, 4795-4797.
13. M. Hariharan, Y. Zheng, H. Long, T. A. Zeidan, G. C. Schatz, J. Vura-Weis, M. R. Wasielewski, X. B. Zuo, D. M. Tiede and F. D. Lewis, *J. Am. Chem. Soc.*, 2009, **131**, 5920-5929.
14. P. P. Neelakandan, Z. Pan, M. Hariharan, Y. Zheng, H. Weissman, B. Rybtchinski and F. D. Lewis, *J. Am. Chem. Soc.*, 2010, **132**, 15808-15813.
15. T. M. Wilson, T. A. Zeidan, M. Hariharan, F. D. Lewis and M. R. Wasielewski, *Angew. Chem. Int. Ed.*, 2010, **49**, 2385-2388.
16. T. Seki, S. Yagai, T. Karatsu and A. Kitamura, *J. Org. Chem.*, 2008, **73**, 3328-3335.
17. W. Wang, L. S. Li, G. Helms, H. H. Zhou and A. D. Q. Li, *J. Am. Chem. Soc.*, 2003, **125**, 1120-1121.
18. J. J. Han, A. D. Shaller, W. Wang and A. D. Q. Li, *J. Am. Chem. Soc.*, 2008, **130**, 6974-6982.
19. R. Carmieli, T. A. Zeidan, R. F. Kelley, Q. Mi, F. D. Lewis and M. R. Wasielewski, *J. Phys. Chem. A*, 2009, **113**, 4691-4700.
20. N. Rahe, C. Rinn and T. Carell, *Chem. Commun.*, 2003, 2120-2121.
21. T. A. Zeidan, R. Carmieli, R. F. Kelley, T. M. Wilson, F. D. Lewis and M. R. Wasielewski, *J. Am. Chem. Soc.*, 2008, **130**, 13945-13955.
22. C. Wagner and H.-A. Wagenknecht, *Org. Lett.*, 2006, **8**, 4191-4194.
23. F. D. Lewis, L. Zhang, X. Liu, X. Zuo, D. M. Tiede, H. Long and G. C. Schatz, *J. Am. Chem. Soc.*, 2005, **127**, 14445-14453.
24. M. McCullagh, M. Hariharan, F. D. Lewis, D. Markovitsi, T. Douki and G. C. Schatz, *J. Phys. Chem. B*, 2010, **114**, 5215-5221.
25. D. Baumstark and H.-A. Wagenknecht, *Angew. Chem. Int. Ed.*, 2008, **47**, 2612-2614.
26. F. Menacher and H.-A. Wagenknecht, *Photochem. Photobiol. Sci.*, 2011, **10**, 1275-1278.
27. G. Bonner and A. M. Klibanov, *Biotechnol. Bioeng.*, 2000, **68**, 339-344.
28. W. Wang, W. Wan, H. H. Zhou, S. Q. Niu and A. D. Q. Li, *J. Am. Chem. Soc.*, 2003, **125**, 5248-5249.
29. R. L. Letsinger and T. Wu, *J. Am. Chem. Soc.*, 1995, **117**, 7323-7328.
30. V. L. Malinovskii, D. Wenger and R. Haner, *Chem. Soc. Rev.*, 2010, **39**, 410-422.
31. C. R. Cantor and P. R. Schimmel, *Biophysical Chemistry*, W. H. Freeman, New York, 1980, vol. 2, pp. 418-425.
32. T. Heek, C. Fasting, C. Rest, X. Zhang, F. Wurthner and R. Haag, *Chem. Commun.*, 2010, **46**, 1884-1886.
33. T. E. Cheatham, P. Cieplak and P. A. Kollman, *J. Biomol. Struct. Dyn.*, 1999, **16**, 845-862.
34. T. A. D. D. A. Case, I. Cheatham, T. E., C. L. Simmerling, J. Wang, R. E. Duke, R. Luo, R. C. W. M. Crowley, W. Zhang, K. M. Merz, B. Wang, S. Hayik, A. Roitberg, G. Seabra, I. K. F. W. Kolossváry, F. Paesani, J. Vanicek, X. Wu, S. R. Brozell, T. Steinbrecher, H. Gohlke, C. T. L. Yang, J. Mongan, V. Hornak, G. Cui, D. H. Mathews, M. G. Seetin, C. Sagui, V. Babin and P. A. Kollman, Amber 10. University of California: San Franscisco, 2008.
35. Z. E. X. Dance, Q. Mi, D. W. McCamant, M. J. Ahrens, M. A. Ratner and M. R. Wasielewski, *J. Phys. Chem. B*, 2006, **110**, 25163-25173.
36. B. Rybtchinski, L. E. Sinks and M. R. Wasielewski, *J. Phys. Chem. A*, 2004, **108**, 7497-7505.